CML

Computer Mechanics Laboratory

Technical Report No. 03-005

THE EFFECTS OF E-BLOCK ARM EDGE SHAPE ON AIRFLOW AND SLIDER OFF-TRACK VIBRATION IN A MODELED HARD DISK DRIVE

Toru Watanabe
HDD Division, Fujitsu Ltd.
4-4-1 Kamikodanaka, Nakahara-ku,
Kawasaki, 211-8588, Japan

Hany M. Gross, David B. Bogy, and Ömer Savas
Computer Mechanics Laboratory
Department of Mechanical Engineering
University of California, Berkeley 94720-1740

January 2003

Abstract

The shape of the trailing or leading edge of an E-block arm was modified from a rectangular cross section to a finned or round shape using adhesive tape. The airflow around the arm tip was measured for the different leading and trailing edges using a constant-temperature hot-wire anemometer, and the slider off-track vibration was measured using a laser Doppler vibrometer (LDV). In the airflow measurements a peak around 4 kHz was observed for all arm shapes in the power spectra of the flow fluctuation. The minimum magnitude of this peak was observed for the round edge shape while for the fin type, the peak was the highest. The slider off-track vibration was compared for both leading and trailing edge shapes. For the round edge geometry, a 10% reduction in the total root mean square (rms) amplitude was obtained in the 2-20 kHz range as compared to the reference arm.

Table of Contents

List of Figures

1. Introduction

Hard disk drives (HDD's) face constant demands for higher recording density, faster data transfer rates and higher reliability. In order to obtain a higher recording density, the track pitch must be reduced. In addition, the disk rotation speed has been increased to reduce rotational latency in high performance drives. At such high rotation disk speeds, high aerodynamic forces on the suspension and the E-block arm are caused by the airflow between the disks. This drag force makes steady head positioning difficult in high rotation speed drives. Therefore, reducing the drag forces on the suspension and the E-block arm is essential for high performance disk drives.

In a well-known study of the effect of airflow on the suspension vibration, Yamaguchi *et al.* [1] found that the amplitude of the suspension vibration was proportional to the square of the air velocity approaching the suspension. In their subsequent paper [2, 3], they investigated the flow using hot-wire anemometer measurements and numerical simulations. They showed that the suspension vibration was linked to the air fluctuation downstream of the suspension. They found that suspension vibration can be reduced by using an airfoil shape for the suspension cross-section.

It is also important to understand the airflow between co-rotating disks for reducing suspension vibration. The airflow between co-rotating disks with a full cylindrical shroud was numerically simulated by Iglesias *et al.* [4]. They predicted significant vertical velocity fluctuations, which caused disk flutter, at the outer regions of

the disk. However, their model did not include the arms and suspensions needed to move the heads to the desired track. Therefore the effects of the arm on the airflow between disks still needed to be investigated. Abrahamson *et al.* [5] performed flow visualizations using a dye method in a more realistic disk drive model, but again without head gimbal assemblies (HGA's). They observed vortex shedding from the arm tip. But their test configuration had arms of the type used with older linear actuators with the slider rails perpendicular to the suspension. In recent drives the sliders are in-line with the suspensions and arms for high access speeds. Flow visualization for the in-line configuration drive was carried out by Girard *et al.* [6]. They observed vortex shedding around the E-block arm tip, which originated from the flow along the leading edge and the trailing edge of the arm.

Gross *et al.* [7, 8] experimentally investigated the effects of E-block arm thickness on the off-track vibration of the read/write head and the airflow downstream of the arm tip in a modeled HDD. They showed a correlation between the head off-track vibration and the rms dynamic head fluctuation downstream of the arm tip.

Generally, flow induced vibration depends on the shape of a body. It is well known through experimental investigation that a body with a rectangular cross-section experiences a high drag force. In this paper, the results of an experimental investigation of the effects of various edge shapes on slider off-track vibration and airflow around the arm tip are presented.

2. Experimental Measurements

2.1. Modeled Hard Disk Drive

A modeled HDD was designed and built for this study as shown in Fig. 1(a). The arm is not actuated, but is fixed to base plate A by a screw. The spindle, which is an actual drive ball bearing spindle, and the shroud are installed on base plate B. A cross plate is used to support the top end of the spindle (Fig. 1(b)). Base plate B can be rotated around an axis corresponding to the actual pivot of the E-block, in order to seek different radial positions. Two 84 mm diameter aluminum disks were stacked on the spindle with a 2 mm spacer in between, and the spindle was operated at 10 krpm. In this study, the head position was fixed at the inner diameter (ID) position, and the E-block arm was inserted between the two disks with no HGA's attached to it.

2.2. Flow Measurement

A customized hot-wire probe (TSI model 1276CF-10A) was used for measuring the flow field. The body length of the probe was extended, so that it could be inserted between the two disks. The probe diameter was 0.9 mm and the sensor length 0.2 mm, which is 10% of disk separation. The sensor was oriented perpendicular to the disk surfaces. Therefore, the sensor was most sensitive to the in-plane flow velocity component. The mean flow velocity, rms flow fluctuation, and flow fluctuation power spectra were computed using a spectrum analyzer (model HP3563A). The measurement locations are shown in Fig. 2, which corresponds to the top view of Fig. 1(a).

2.3. Slider Off-Track Vibration Measurement

The E-block arm with two HGA's was inserted between the two disks, and the slider off-track vibration was measured during disk rotation using LDV. Two methods were used for evaluating the vibration measurements. The first was the power spectrum, and the second the total rms amplitude that was given by a summation of the power spectrum in a certain frequency range. If an rms power spectrum is expressed by $P_{rms}(f)$ as a function of frequency, f, then the total rms amplitude, A_{rms}, can be written as

$$A_{rms} = \sqrt{h \sum_i P_{rms}(f_i)}, \tag{1}$$

where h is a scale factor for the windowing function. A Hanning window was used in these measurements. The scale factor h is 2/3 for a Hanning window in the HP3563A. It should be noted that the relationship expressed in Eq. (1) is a Pythagorian relationship, and that it applies for different frequency ranges. The tested suspensions did not have the usual side rails or ribs on the loadbeam. Photographs of the head stack assembly (HSA) and the HGA used are shown in Fig. 3.

2.4. Arm Edge Shapes

The arm shapes at the leading and trailing edges were modified using adhesive tape. The thickness of the arm was 1.0 mm. The formed shapes are shown in Fig. 4. Each arm type is named as shown in the figure. The arm thickness is increased at the attached tape area due to the thickness of the adhesive tape, which is approximately 0.05 mm, giving a total thickness of 1.1 mm. The T11 type is the reference for comparison of the other arm edge shapes, since it has the same total thickness of 1.1 mm as the modified arms.

3. Results and Discussion

3.1. Data Analysis

The flow speed, u, in turbulent flow analysis is commonly expressed as the sum of the mean and fluctuating components of the speed, $\hat{u}$ and u', respectively

$$u = \hat{u} + u' . \tag{2}$$

The rms flow fluctuation, u_{rms}, can be computed from the spectrum analyzer output of the power spectrum $\overline{G_{u'}(f)}$ of the flow fluctuation, where f denotes frequency, according to[1]

$$u_{rms} = \sqrt{a \sum_i \overline{G_{u'}(f_i)}}, \tag{3}$$

where a is a scale factor for the windowing function used in calculating the power spectra. A Hanning window was employed in this study, for which $a = 2/3$.

The rms flow fluctuation is usually expressed as a percentage of the local mean flow speed. This percentage is known as the turbulence intensity, TI, of the flow, and it was computed at each measurement point according to

$$TI = \frac{u_{rms}}{\bar{u}} . \tag{4}$$

The drag force, D, on a body can be expressed as

[1] Eq. (3) is based on Parseval's theorem, which states that for an aperiodic function $x(t)$ whose Fourier transform is $X(w)$,

$$\int_{-\infty}^{\infty} x^2(t)dt = 2p \int_{-\infty}^{\infty} |X(w)|^2 dw$$

$$D = \int_A C_D q dA, \tag{5}$$

where C_D, A, and q denote the sectional drag coefficient, the projection of the area of the body onto the flow direction, and the dynamic pressure, respectively. The dynamic pressure, q, is given by

$$q = \frac{1}{2} \rho u^2, \tag{6}$$

where ρ denotes air density and u denotes flow speed.

Substituting Eq. (2) into Eq. (6), we may express q as

$$\begin{aligned} q &= \frac{1}{2} \rho \left(\bar{u} + u'\right)^2 \\ &= \frac{1}{2} \rho \left(\left(\bar{u}\right)^2 + 2\bar{u}u' + \left(u'\right)^2 \right) \end{aligned} \tag{7}$$

Similar to velocity, dynamic pressure can be expressed in terms of its mean and fluctuating components, $\bar{q}$ and q', respectively, as

$$q = \bar{q} + q'. \tag{8}$$

It follows from Eqs. (6) through (8) that

$$\bar{q} = \frac{1}{2} \rho \left(\left(\bar{u}\right)^2 + \overline{\left(u'\right)^2} \right), \tag{9}$$

and

$$q' = \frac{1}{2} \rho \left(2\bar{u}u' + \left(u'\right)^2 - \overline{\left(u'\right)^2} \right). \tag{10}$$

If $\hat{u}$ is much greater than $|u'|$, $\bar{q}$ will be dominated by the first term in the brackets of Eq. (9), and q' will be dominated by the first term in the brackets of Eq. (10), and they may be expressed approximately as

$$\bar{q} \approx \frac{1}{2} \rho \left(\bar{u}\right)^2, \tag{11}$$

and

$$q' \approx \rho \bar{u} u'. \tag{12}$$

The rms dynamic pressure fluctuation q_{rms} can now be written as

$$q_{rms} \approx \rho \bar{u} u_{rms}. \tag{13}$$

Consequently, the mean drag force $\overline{D}$ and the rms drag force D_{rms} can be approximated as

$$\overline{D} \approx \frac{1}{2} \int_A C_D \rho \left(\bar{u}\right)^2 dA, \tag{14}$$

and

$$D_{rms} \approx \int_A C_D \rho \bar{u} u_{rms} dA. \tag{15}$$

It is clear from Eqs. (9) and (10) that a higher rms flow fluctuation translates directly into a higher average drag force $\overline{D}$, and a higher rms drag force fluctuation D_{rms}. Eq. (15) also highlights the relevance of the quantity $\hat{u} u_{rms}$, since D_{rms} is approximately proportional to $\hat{u} u_{rms}$. Kim *et al.* [9] showed, through experimental investigation, a correlation between HGA vibration and $\hat{u} u_{rms}$.

The quantities $\bar{h}$ and h_{rms}, defined by,

$$\bar{h} = \frac{1}{2}\left((\bar{u})^2 + (u_{rms})^2 \right) \approx \frac{1}{2}(\bar{u})^2 \qquad (16)$$

and

$$h_{rms} \approx \bar{u} u_{rms} . \qquad (17)$$

will henceforth be loosely referred to as the mean dynamic head and the rms dynamic head fluctuations[2], respectively.

The disk surface speed V_d is given by

$$V_d = \omega r , \qquad (18)$$

where ω is the disk angular speed.

3.2. Mean Flow Speed and rms Flow Fluctuation

Figure 5 shows color contour plots of the disk surface speed. There are two scales in the figure. The first color scale is an automatic scale that shows the full range of the circumferential speed of the disk (Fig. 5(a)). The second color scale is a clipped color scale that is used in all subsequent plots to allow for comparison of the results for the different cases considered (Fig. 5(b)). The upper limit in this scale is based on the maximum mean flow speed measured with the E-block arms inserted between the disks. In these figures, the disk rotates clockwise, and the outlines of the HGA are indicated with dashed lines for reference. It should be noted that these flow measurements were conducted without the HGA's attached to the E-block arm. These views are similar to

[2] Strictly speaking, these quantities should be divided by the gravitational constant $g = 9.81\ m/s^2$ to yield the mean and rms dynamic head.

Fig. 2, but are slightly rotated. The area depicted is in the range of x = 2 to 12 mm and y = -4 to 5 mm of Fig. 2.

The contour plots of both the mean flow speed and the rms flow fluctuation for the T11, Round and Fin types are shown in Figs. 6, 7, and 8, respectively. There is a high mean flow speed region along the upper edge of the HGA outline, and below that region there is a steep gradient region in all cases. The high mean flow speed regions spread along the circumference of the disk. Relatively slow mean flow speed regions are also observed which are caused by the presence of the arm. Most of the upstream flow is prevented from passing over the arm, and the flow direction is forcibly veered along the arm sidewall. Consequently the pressure downstream of the arm is expected to be relatively low. This low-pressure region must be the cause of the flow that comes from outside the disks downstream of the arm as shown in the flow visualizations by Girard *et al.* [6]. The mean flow speed is quite low in comparison with the disk surface speed as shown in the contour plots. On the other hand, the flow obstructed by the arm steers around the arm tip and finally separates from the arm tip. This feature causes the steep gradient region in the flow, which is similar to the shear layer observed in free turbulent flow [10], which is characterized by high velocity fluctuations. It should be noted that the high fluctuation regions appear to be scattered due to the interpolation of sparse data, since the measurement grid is coarser in the horizontal direction than the vertical direction, as shown in Fig. 2. However, the high fluctuation region exhibits the characteristics of a classical shear layer in all cases.

Comparing results for the different arm types, it is evident that the tendencies of the flow patterns are quite similar. Both maxima of the mean flow speed and the rms flow fluctuation for the Fin type are larger than those of the other types. The overextending fins are likely to induce larger separation bubbles, hence, higher mean flow speed and rms flow fluctuation around the arm tip. Focusing on the bottom right hand side of the figures, we see that the rms flow fluctuations in the Round and Fin types are lower than in the T11 type, and that the mean flow speeds in the Round and Fin types in the middle right hand side are higher than in the T11 type. This feature in the Round and Fin types might be linked to the decrease in the drag force on the arm.

3.3. Power Spectra of Flow Fluctuation

The power spectra of the hot-wire anemometer outputs are shown in Figs. 12 through 17. Each line indicates the power spectrum at a certain y-position and the color contour of the power spectrum is also included to illustrate its magnitude. Figures 12 through 14 are for x = 2 mm, and Figs. 15 through 17 for x = 4 mm. The low frequency components are dominant in the range of y = 2.5 to 5 mm in all cases. For y = -5 to 2.5 mm, the high frequency components are more pronounced. The peak at 167 Hz is due to the disk runout associated with 10 krpm disk speed. For the T11 and Fin types at x = 2 mm, a peak is observed around 4 kHz. This peak, however, is not clear for the Round type. This peak is a result of the vortex shedding at the arm tip. The frequency of the peak can be correlated from the Strouhal number St according to

$$St = \frac{f_v d}{U} \tag{19}$$

where f_v, d, and U are the vortex shedding frequency (cycles/sec), the characteristic length of the body, and the characteristic speed of the approaching flow, respectively. It is known that the Strouhal number remains approximately constant at St = 0.21 for the free flow over a circular cylinder if the Reynolds number is within the range 10^3 to 10^4 [10]. The Reynolds number for the E-block arm is 1300 based on the arm thickness, d = 1.1 mm, and measured speed near the arm tip, $U \cong$ 20 m/s. Assuming a Strouhal number St = 0.21 for the case at hand, the expected vortex shedding frequency is 3.8 kHz.

3.4. Slider Off-Track Vibration

The HGA's were attached to the E-block arms, and the slider off-track vibration was measured. In this experiment the off-track vibrations of the Back Round (B Round) and Back Fin (B Fin) types were measured in addition to the arms used in the flow measurements. Figure 18 shows the power spectra of slider off-track vibration for different arm types. The resonant frequencies of the head stack assembly for the E-block arm and HGA's have already been obtained using finite element analysis [7]. According to the results presented in [7], the 2.5 kHz, 7.5 kHz, 12 kHz and 13.5 kHz peaks correspond to the following modes: 1^{st} bending of the HGA, sway of the E-block arm, 2^{nd} torsion of the HGA, and sway of the HGA, respectively. The Fin type result is seen to be almost identical to that of the T11 type. It is observed that the Round, B Round and B Fin types have lower peaks than the T11 and the Fin types. The off-track vibration resulting from structural resonances was assessed by evaluating the rms amplitudes of vibration over the frequency range 2-20 kHz. The rms amplitudes were evaluated to determine the effect of the arm edge shape modifications on the vibration. Figure 19 shows the rms

amplitudes for the different arm types over several frequency ranges. We focused on the 2-20 kHz band since it contains the structural resonances of the HSA.

The 2-20 kHz band is divided into three frequency bands: 2-6 kHz, 6-10 kHz and 10-20 kHz bands. The 2-6 kHz band includes the 1st bending mode of the HGA, the 6-10 kHz band is dominated by the E-block arm sway mode, and the 10-20 kHz band contains the 2nd torsion and sway modes of the HGA. The rms component in the 2-6 kHz band for the Fin type is comparable to that of the T11 type. This band contains vortex shedding frequencies as mentioned above. The Fin type has a higher magnitude in the power spectrum of the flow fluctuation, which is a possible explanation for the trend observed in the 2-6 kHz vibration component. The response of the Round type in this band is lower than that of the T11 and Fin types. This may be explained by the observation that the Round type had a lower peak at 4 kHz in the power spectrum of the flow fluctuation.

In the 10-20 kHz band, the differences between the different arms are smaller than in the 2-6 kHz band. In this band, the effect of vortex shedding is quite minor. Since the distribution of the quantity $\hat{u}u_{rms}$ in the HGA region is comparable for the three types, we expect the effect on HGA vibration to be similar. On the other hand, in the 6-10 kHz band, T11 has a higher rms amplitude. This may be explained by the fact that, in general, the flow approaching a rectangular body is prone to separation at the corners of the body at both the upstream and down stream sides, causing a large drag force. The examined modifications of the arm edge were expected to hinder the separation at the corners of the

arm. The results show that these modifications of the arm edge shape can reduce the drag force on the arm.

An examination of the 2-20 kHz range in Fig. 19 indicates that it is possible to reduce slider off-track vibration by modifying the arm edge shape from the basic rectangular cross-section, represented by T11. The best improvements were achieved in the Round and Back Round cases, as the slider off-track vibration was reduced by about 10% (Fig. 19).

4. Conclusion

In this study the effects of arm edge shapes on the flow field and slider off-track vibration were investigated experimentally in a modeled HDD. From the airflow measurements using a hot-wire anemometer, we observed a fluctuation peak at 4 kHz due to vortex shedding. Its magnitude increased when the leading edge shape was modified to the Fin type. Evaluating the product of mean flow speed and rms flow fluctuation, we did not observe significant variation in the HGA region of the flow. Using slider off-track measurements we confirmed the effects of the arm edge shape modifications. By modifying the leading and trailing edges of the arm to be round, we obtained a 10% reduction of the total rms amplitude compared to the T11 type.

5. Acknowledgements

This study was supported by the Computer Mechanics Laboratory at the University of California at Berkeley, the Hard Disk Drive Division at Fujitsu Ltd., and the Information Storage Industry Consortium.

6. References

[1] Yamaguchi, Y., Takahashi, K., Fujita, H. and Kuwahara, K., "Flow Induced Vibration of Magnetic Head Suspension in Hard Disk Drive", IEEE Transaction of Magnetics, Vol. 22, No. 5, September 1986, pp. 1022-1024.

[2] Yamaguchi, Y., Talukder, A.A., Shibuya, T. and Tokuyama, M., "Air Flow Around a Magnetic-Head-Slider Suspension and Its Effect on Slider Flying-Height Fluctuation", IEEE Transaction of Magnetics, Vol. 26, No. 5, September 1990, pp. 2430-2432.

[3] Tokuyama, M., Yamaguchi, Y., Miyata, S. and Kato, C., "Numerical Analysis of Flying-Height Fluctuation and Positioning Error of Magnetic Head due to Flow Induced by Disk Rotation", IEEE Transaction of Magnetics, Vol. 27, No. 6, November 1991, pp. 5139-5141.

[4] Iglesias, I. and Humphrey, J., "Two- and Three-Dimensional Laminar Flows Between Disks Co-Rotating in a Fixed Cylindrical Enclosure", International Journal for Numerical Methods in Fluids, Vol. 26, 1998, pp. 581-603.

[5] Abrahamson, S., Chiang, C. and Eaton, J.K., "Flow Structure in Head-Disk Assemblies and Implications for Design", Adv. Info. Storage Syst., Vol. 1, 1991, pp. 111-132.

[6] Girard, J., Abrahamson, S. and Uznanski, K., "The Effect of Rotary Arms on Corotating Disk Flow", ASME Journal of Fluids Engineering, Vol. 117, June 1995, pp. 259-262.

[7] Gross, H. M., Watanabe, T., and Bogy, D. B., "The Effects of E-Block Arm Thickness on Head Vibration Between Co-Rotating Disks in a Modeled Hard Disk Drive", CML Technical Report, No. 02-018, December 2002.

[8] Gross, H. M., Watanabe, T., Bogy, D. B., and Savas, Ö., "The Effects of E-Block Arm Thickness on the Airflow Downstream of the E-Block Arm in a Modeled Hard Disk Drive", CML Technical Report, No. 03-004, January 2003.

[9] Kim, B.-C. and Mote, C.D., "Suppressing Turbulence Induced Vibration of the Head Suspension Assembly in a Hard Disk Drive", CML Technical Report, No. 99-015, August 1999.

[10] Schlichting, H., "Boundary-Layer Theory", McGraw-Hill, Inc., 6th Edition, 1968.

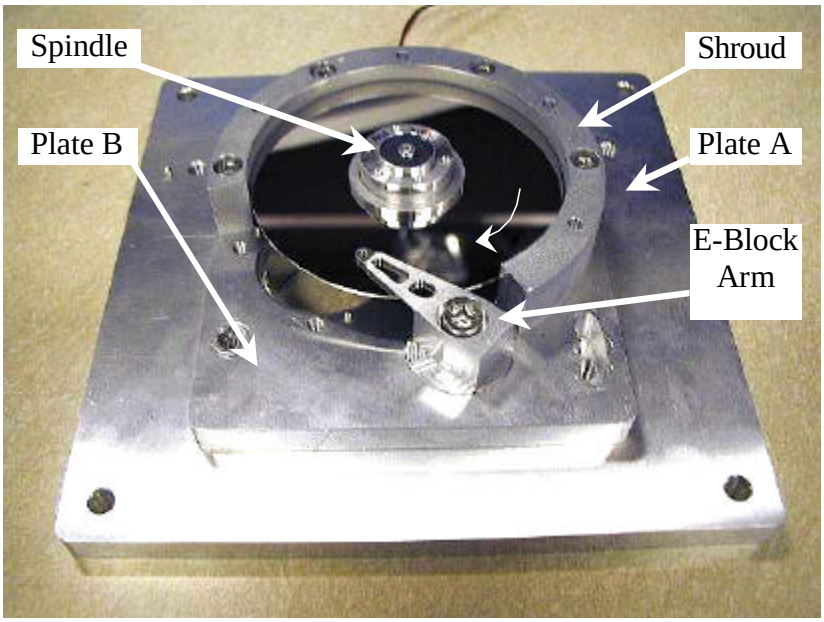

(a) Setup without top disk and cover

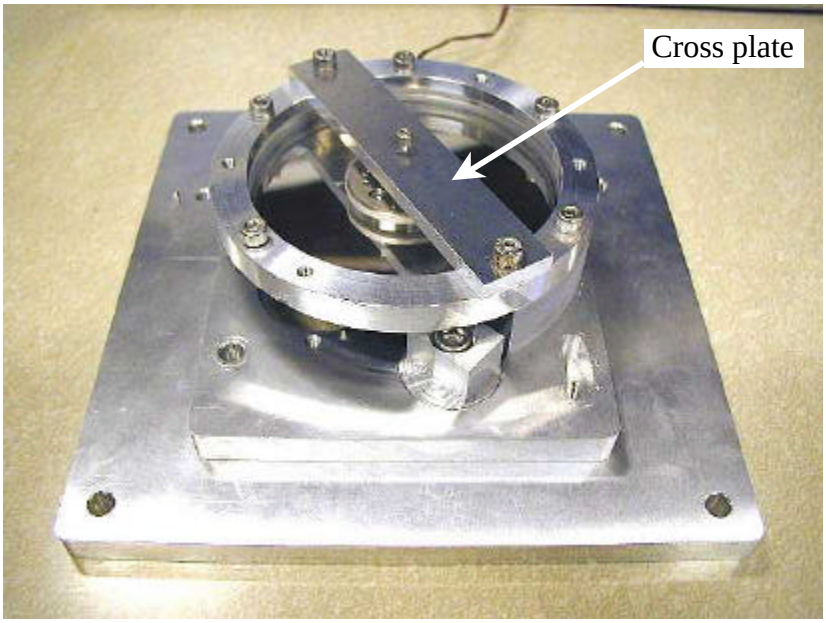

(b) Setup with top disk

Figure 1: Modeled disk drive.

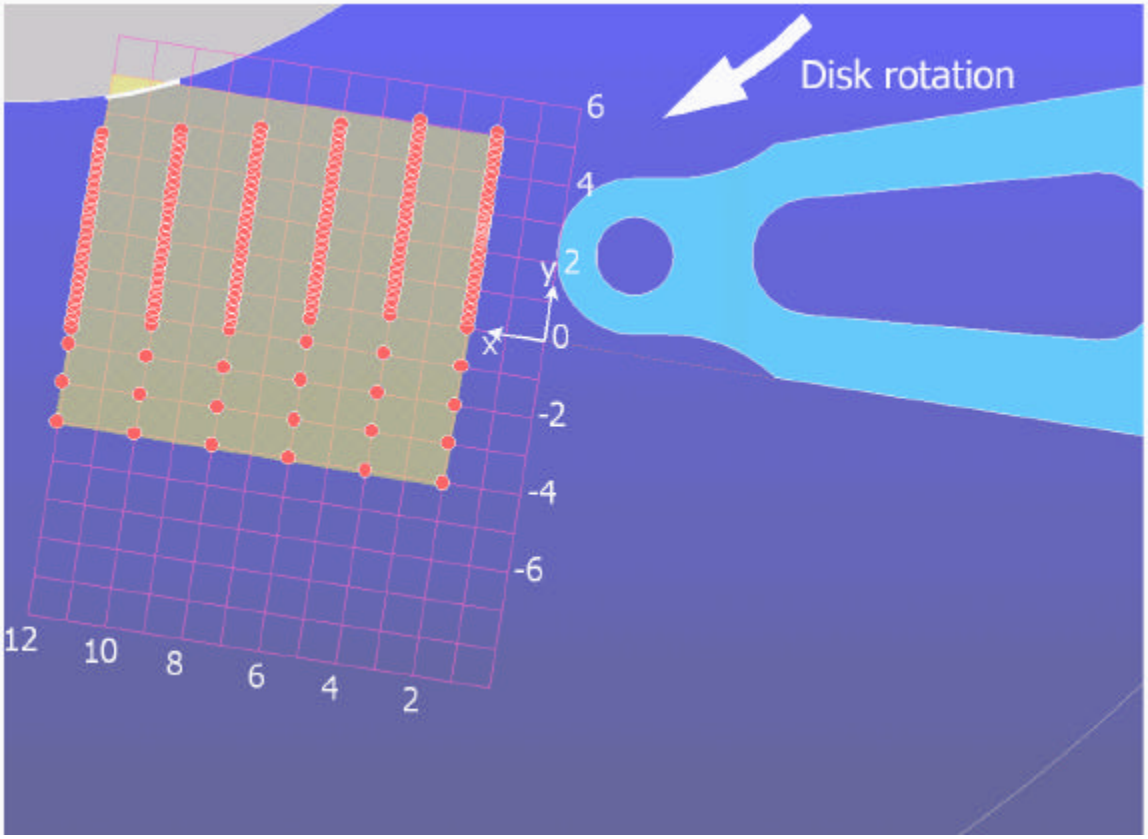

Figure 2: Measurement points (●). Coordinate system is shown in mm.

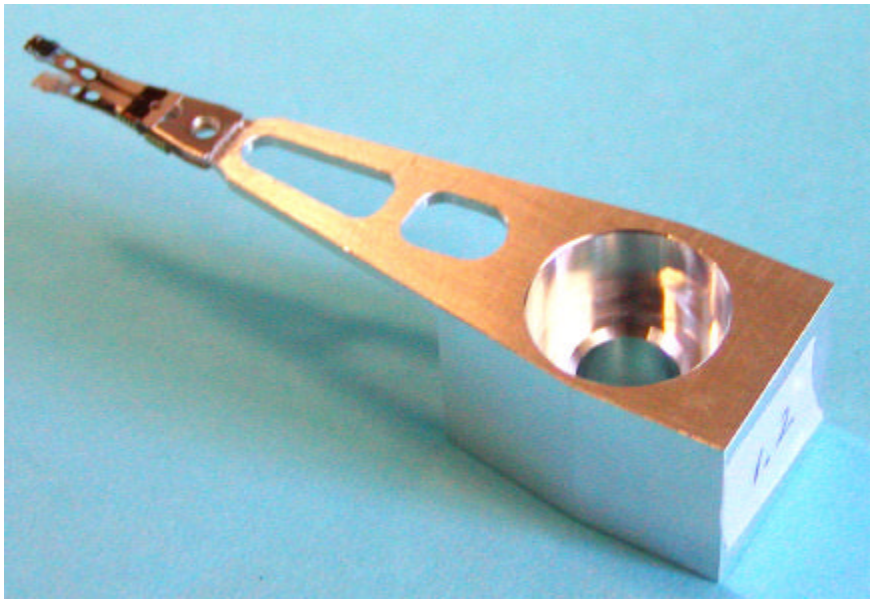

(a) A close-up of the HSA.

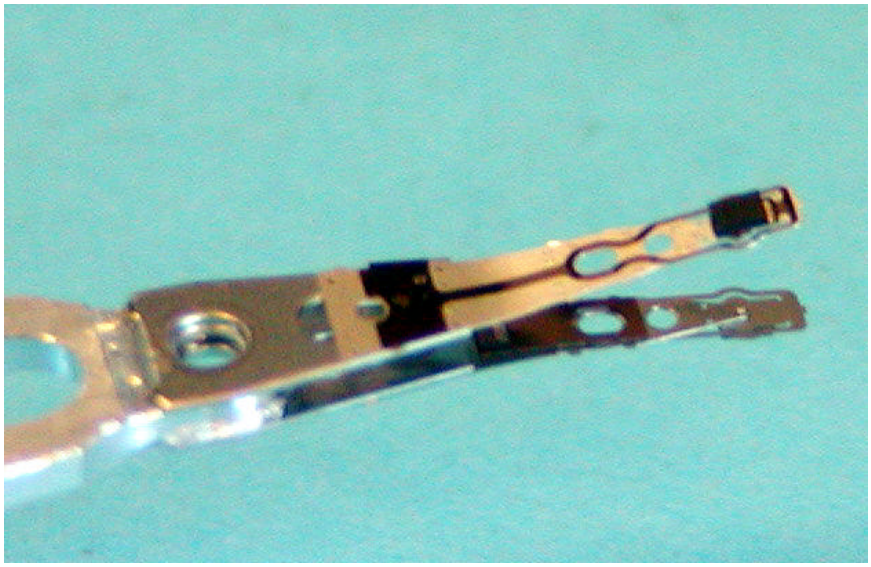

(b) A close-up of the HGA.
Figure 3: HGA and HSA photographs.

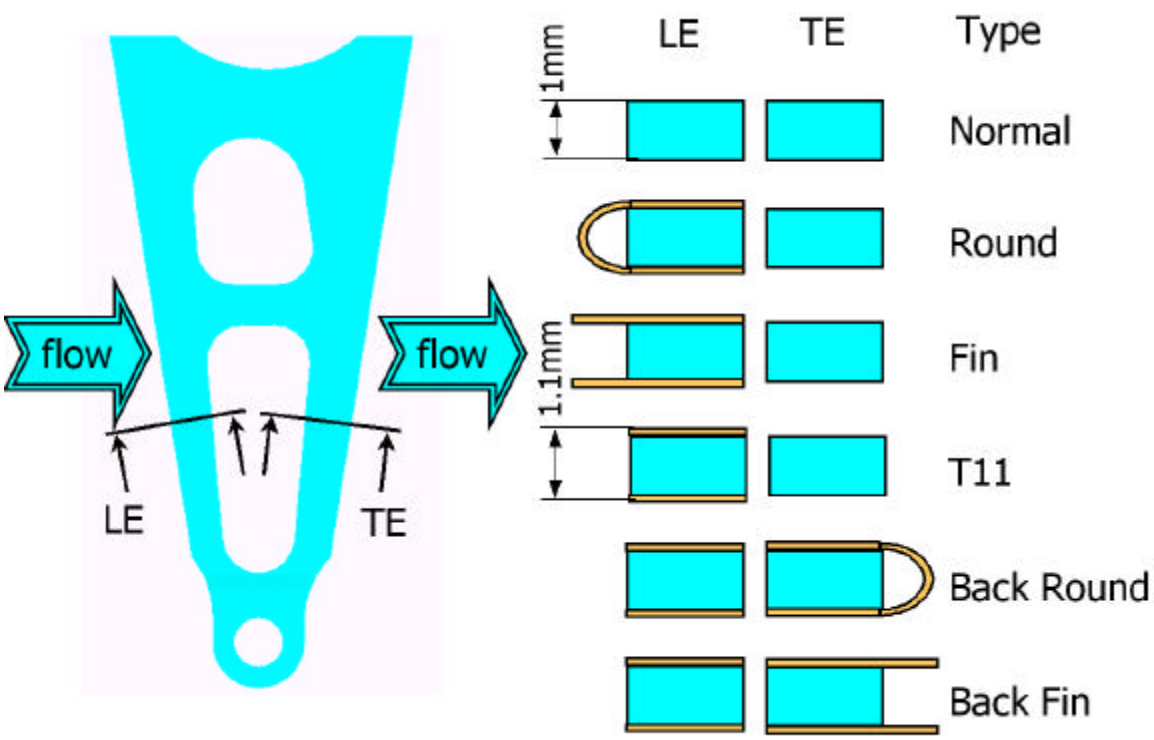

Figure 4: Cross section shapes at the leading edge and the trailing edge.

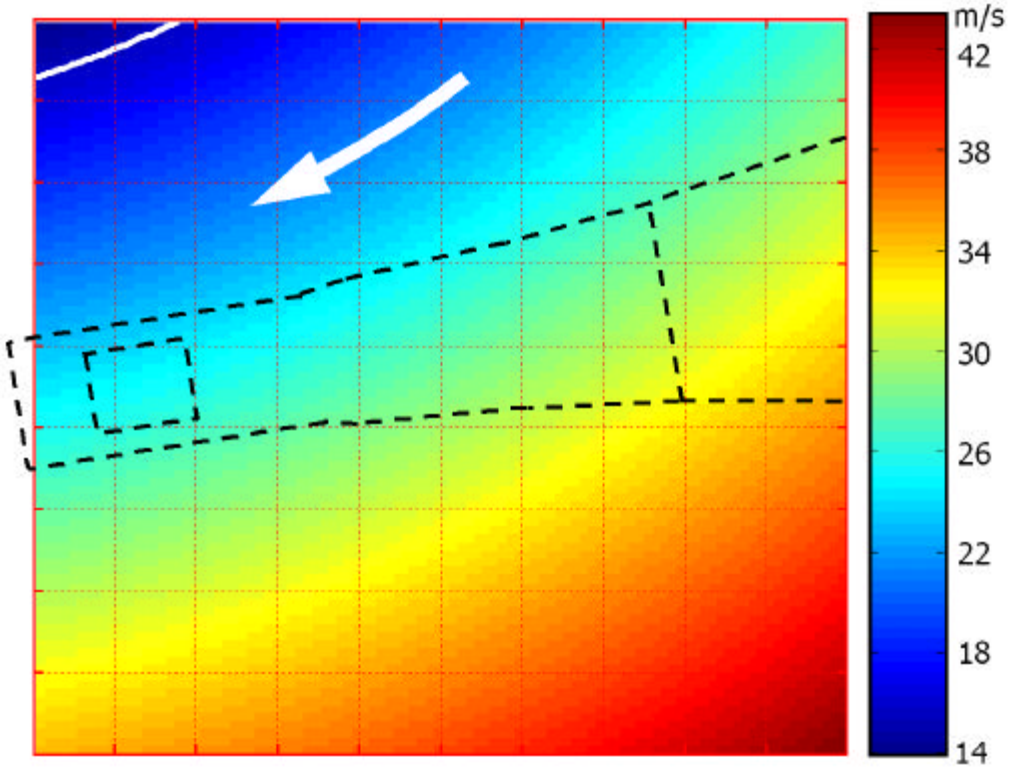

(a) Automatic color scale

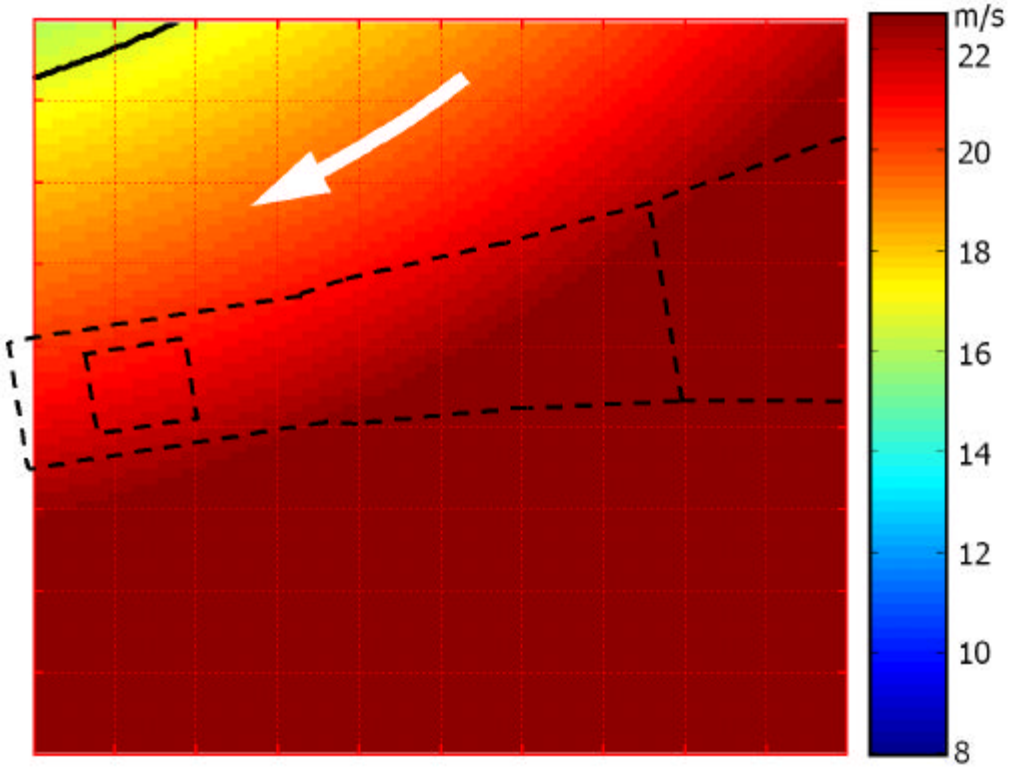

(b) Clipped color scale

Figure 5: Color contour plot of the disk surface speed. Grid scale: 1 mm/div.

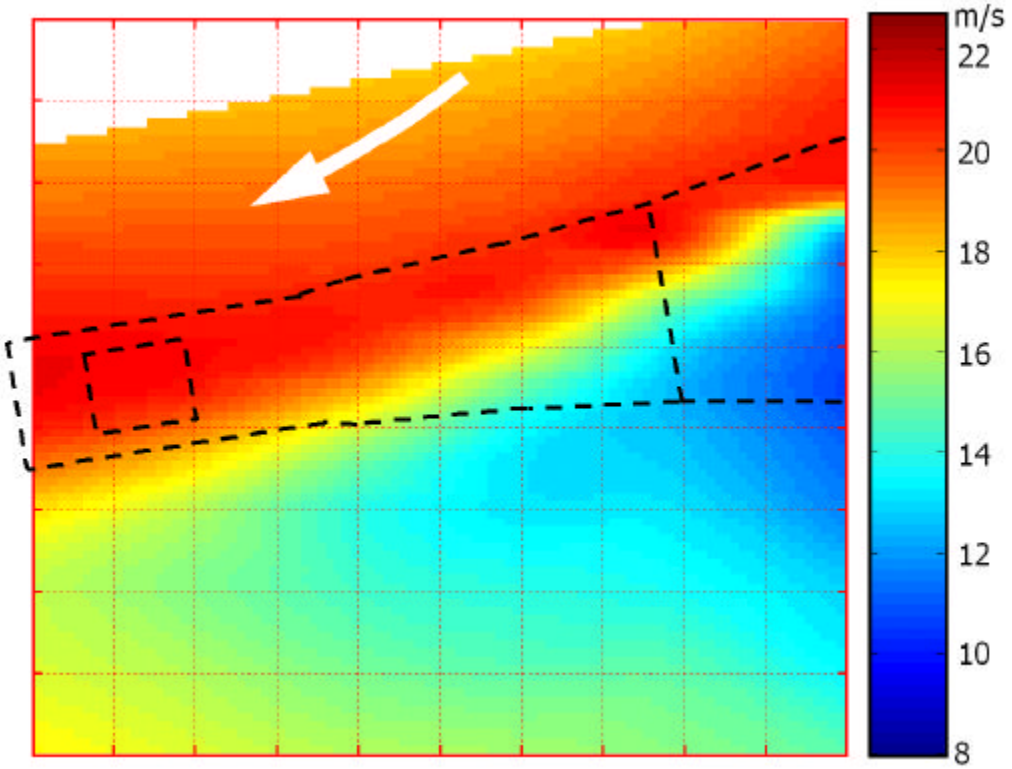

(a) Mean flow speed, $\hat{u}$

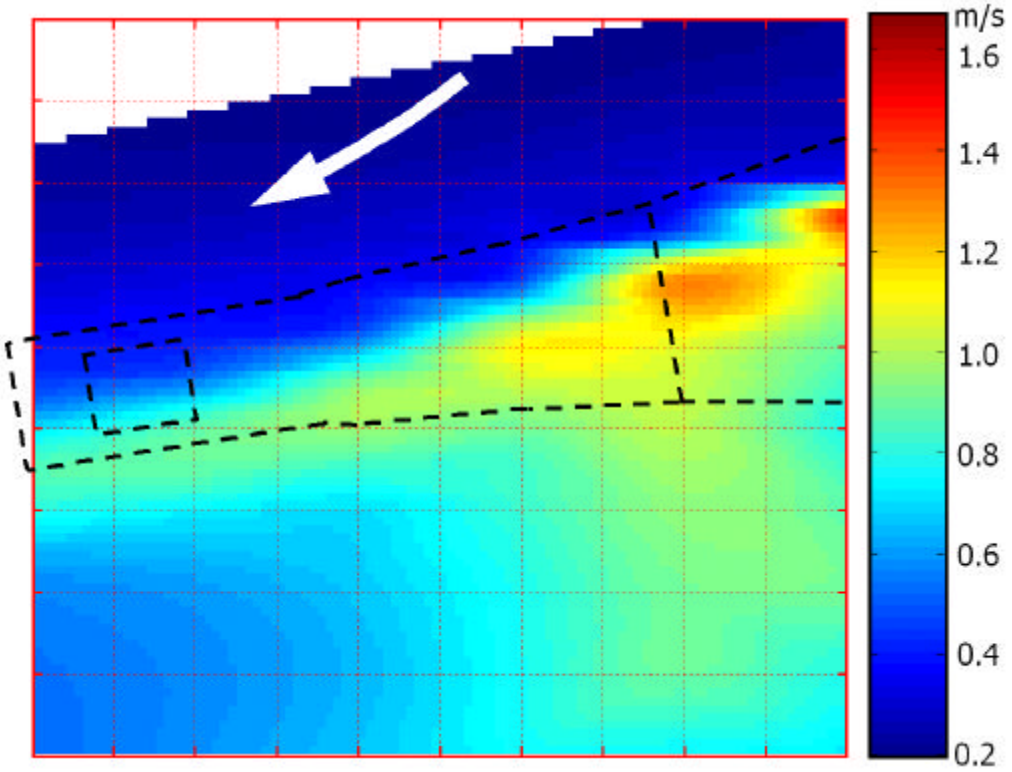

(b) rms flow fluctuation, u_{rms}

Figure 6: Contours of the mean flow speed and rms flow fluctuation for the T11 shape arm. Grid scale: 1 mm/div.

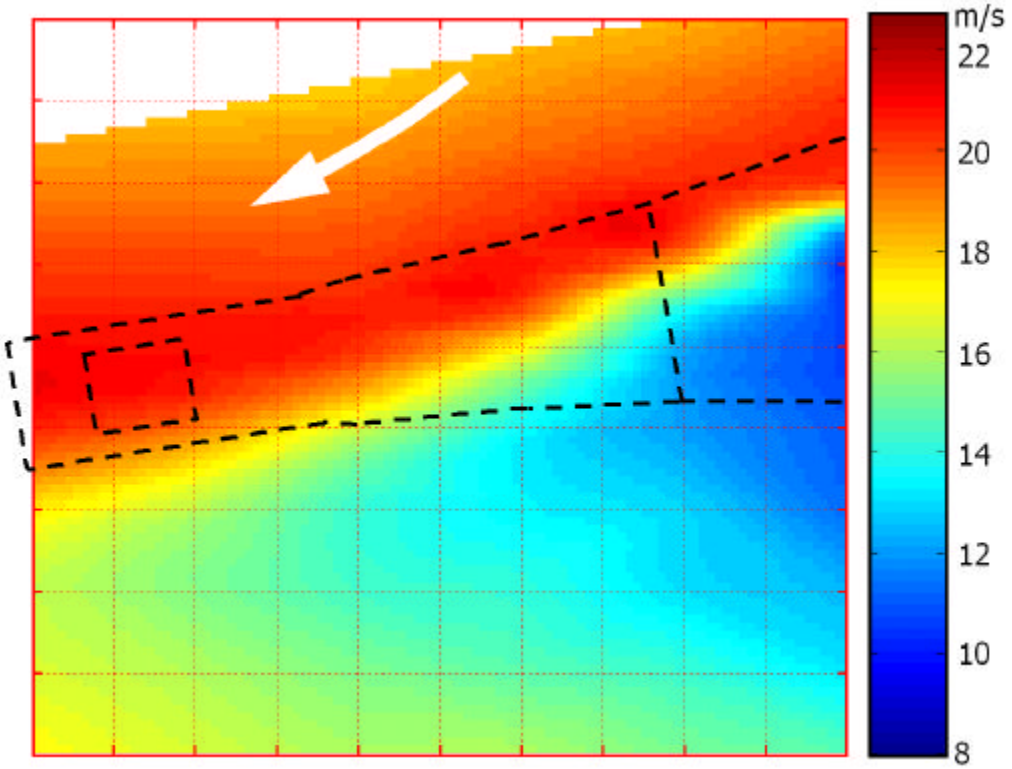

(a) Mean flow speed, $\hat{u}$

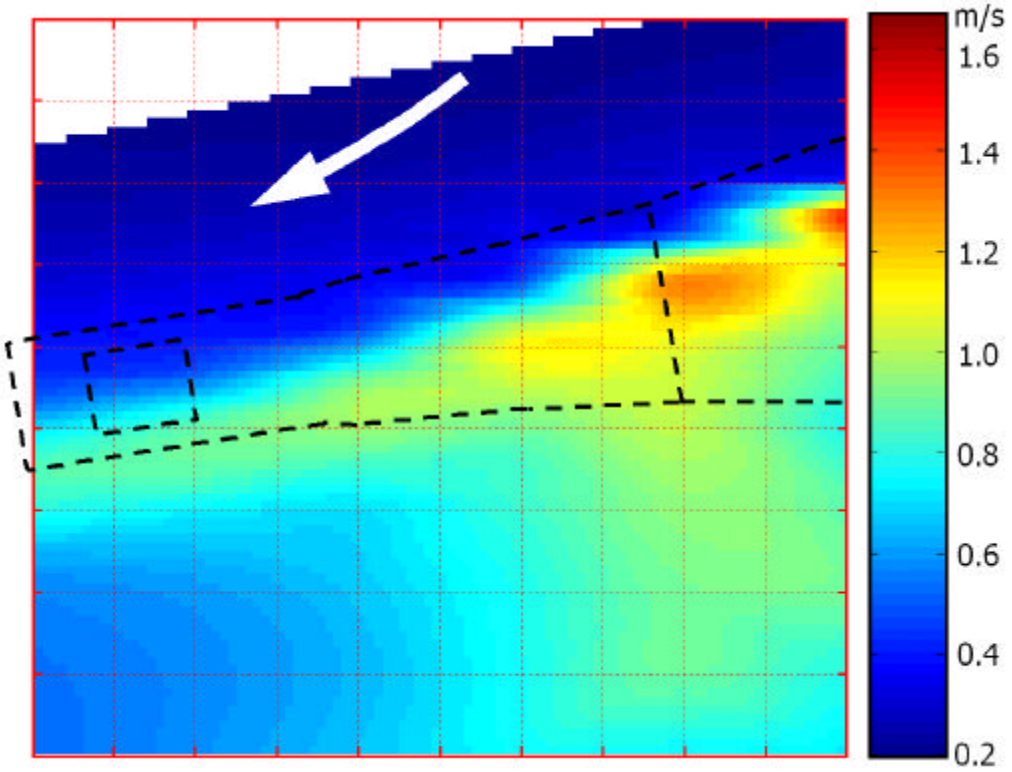

(b) rms flow fluctuation, u_{rms}

Figure 7: Contours of the mean flow speed and rms flow fluctuation for the Round shape arm. Grid scale: 1 mm/div.

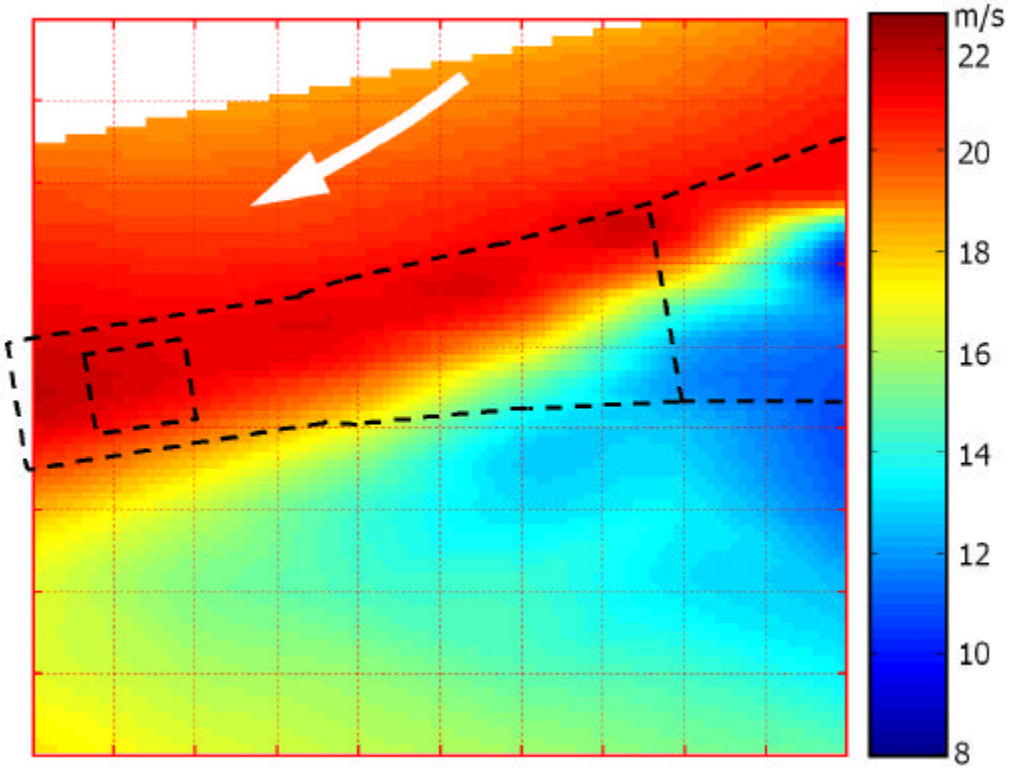

(a) Mean flow speed, $\hat{u}$

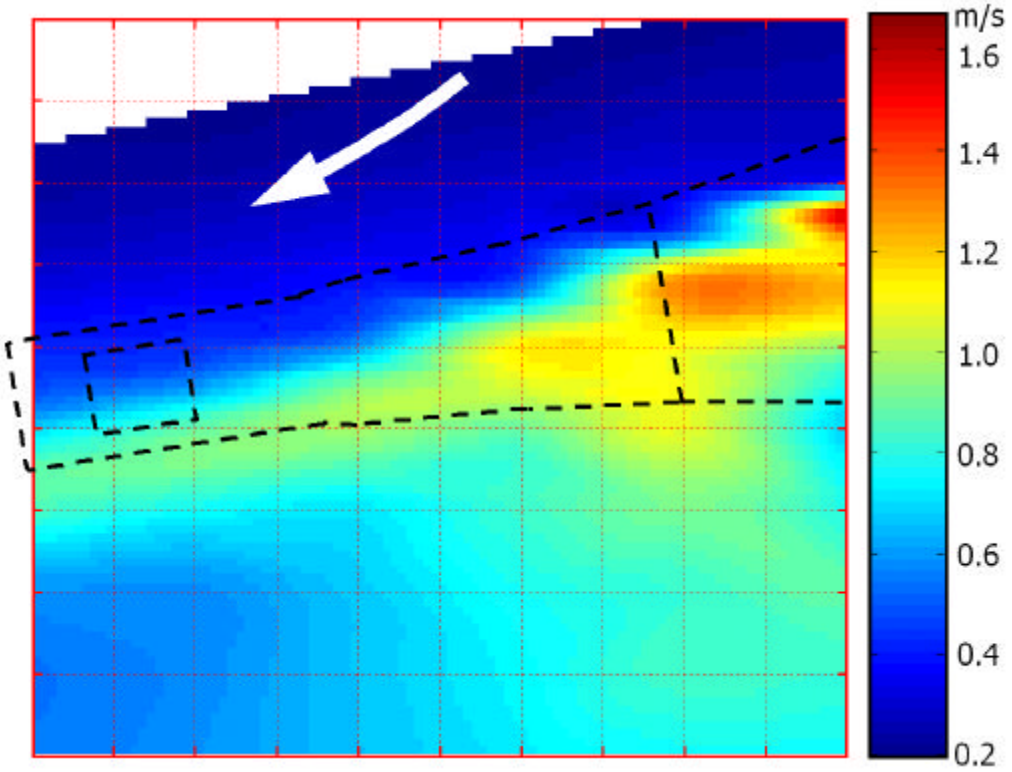

(b) rms flow fluctuation, u_{rms}

Figure 8: Contours of the mean flow speed and rms flow fluctuation for the Fin shape arm. Grid scale: 1 mm/div.

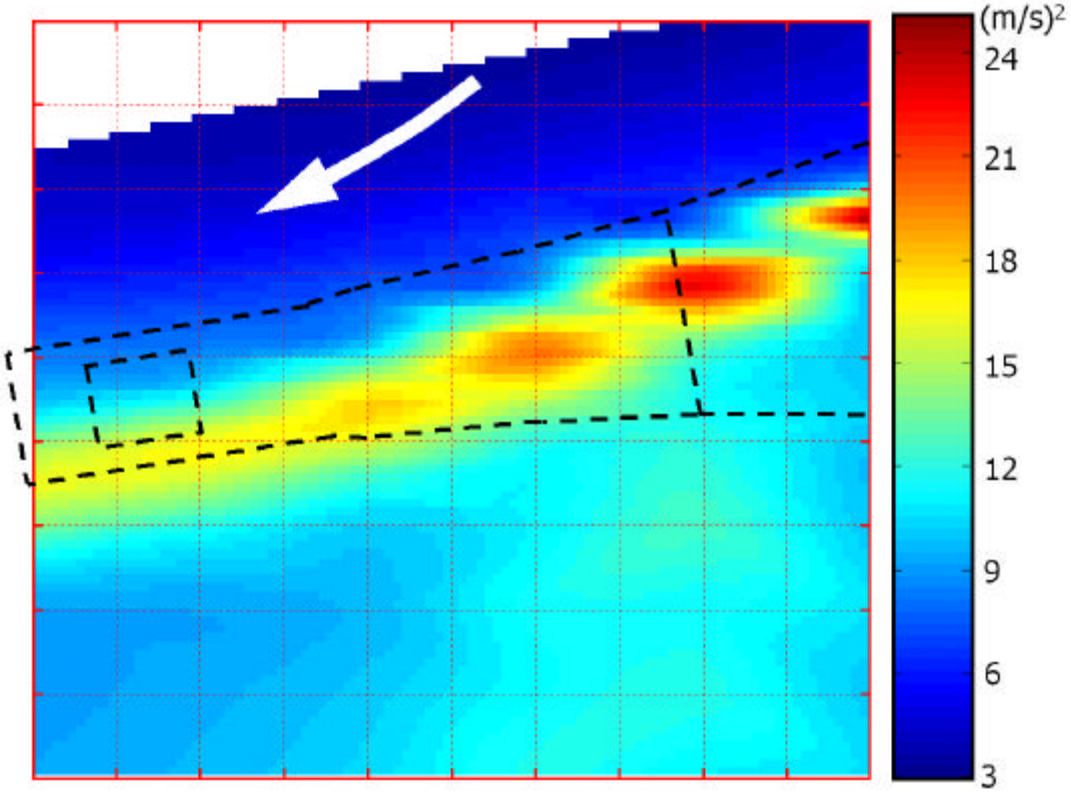

Figure 9: Contours of h_{rms} for the T11 shape arm. Grid scale: 1mm/div.

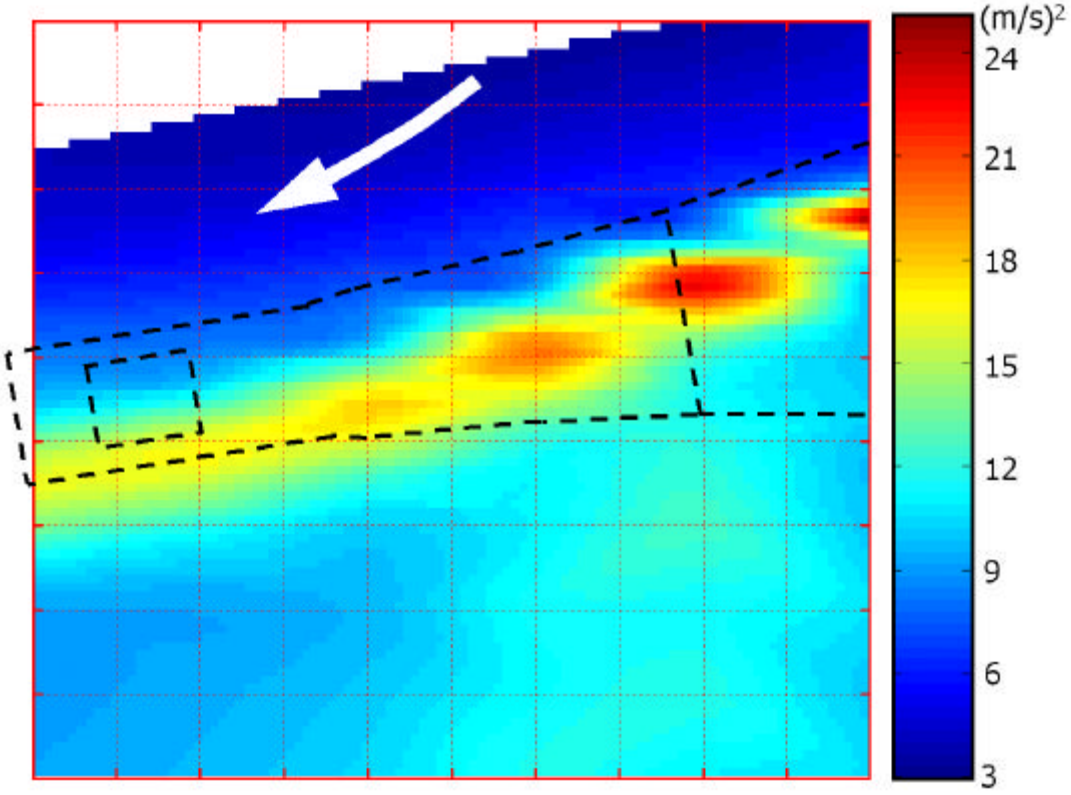

Figure 10: Contours of h_{rms} for the Round shape arm. Grid scale: 1mm/div.

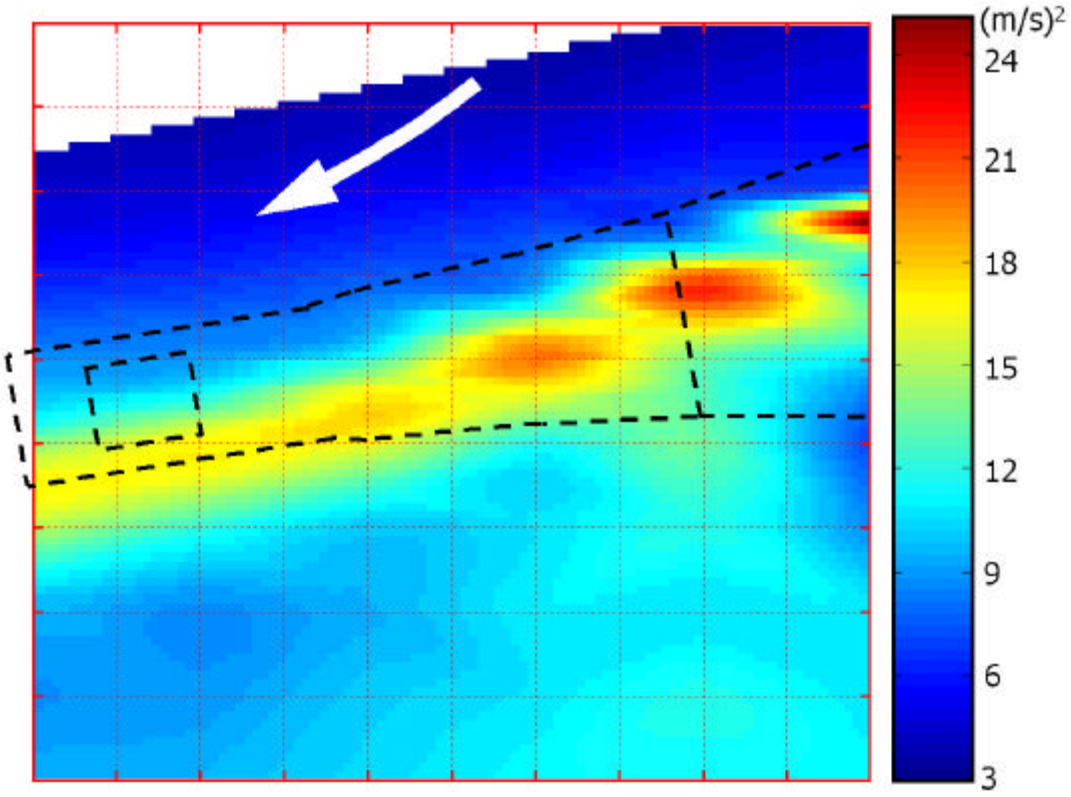

Figure 11: Contours of h_{rms} for the Fin shape arm. Grid scale: 1mm/div.

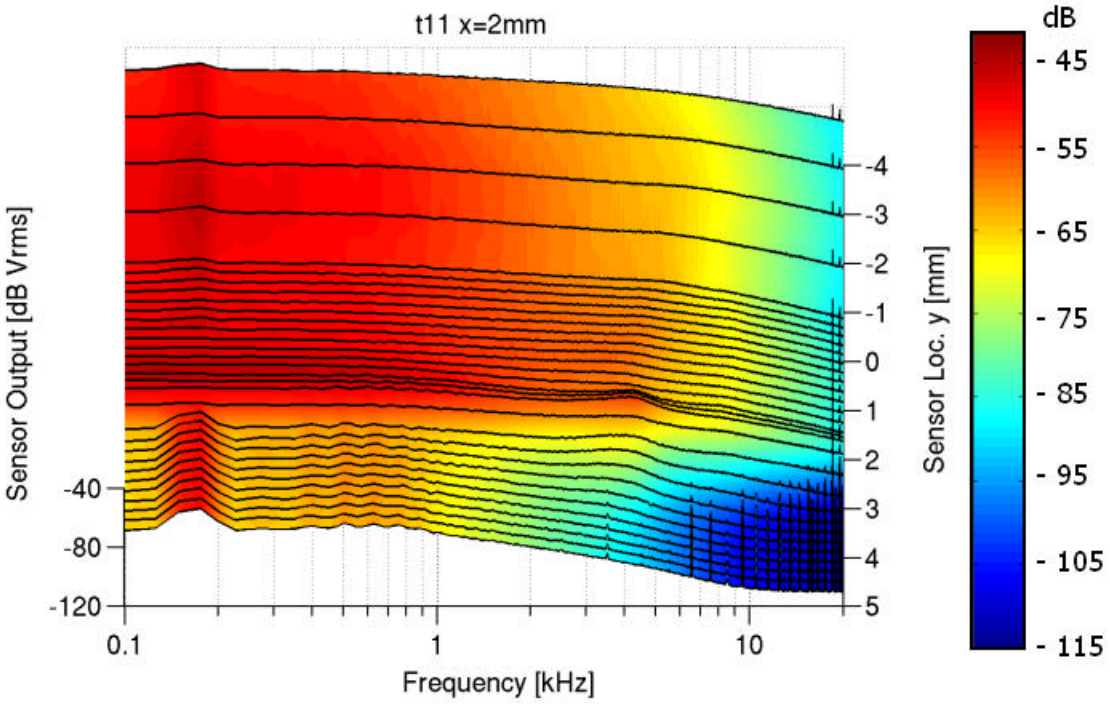

Figure 12: Power spectrum of the hot-wire output for the T11 shape at x = 2 mm.

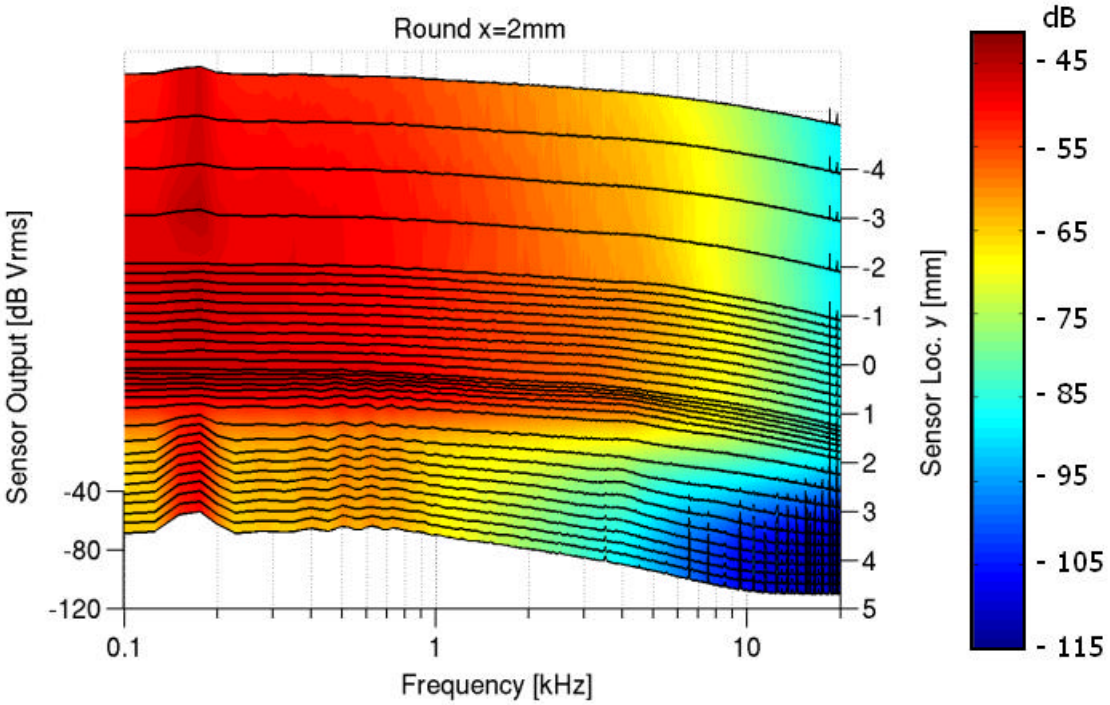

Figure 13: Power spectrum of the hot-wire output for the Round shape at x = 2 mm.

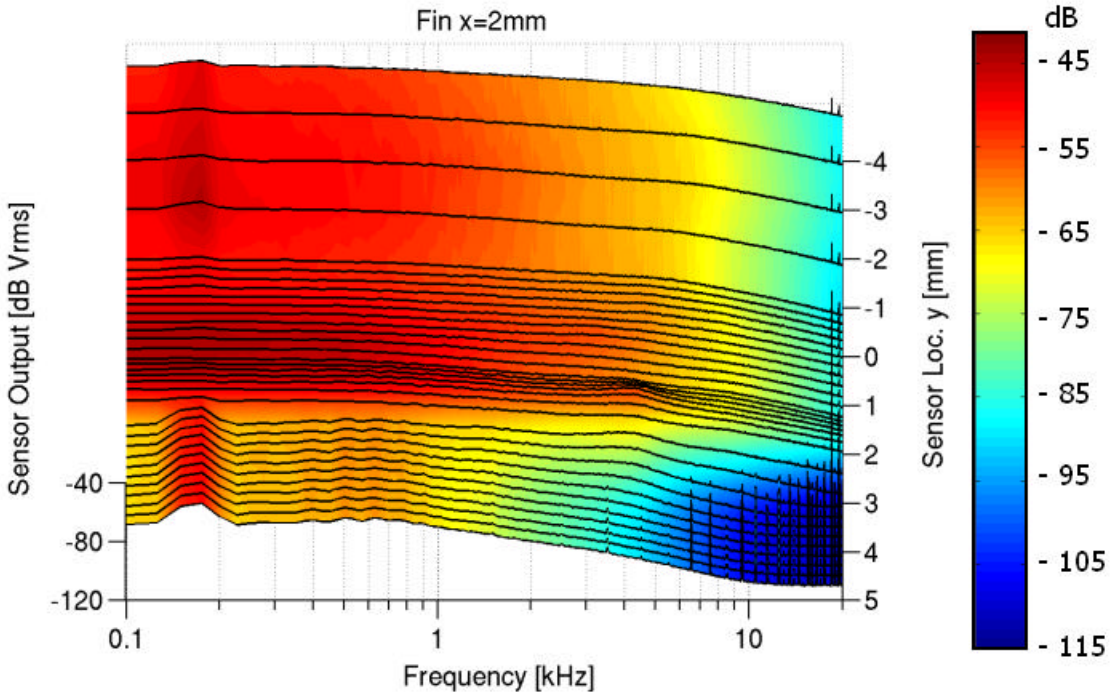

Figure 14: Power spectrum of the hot-wire output for the Fin shape at x = 2 mm.

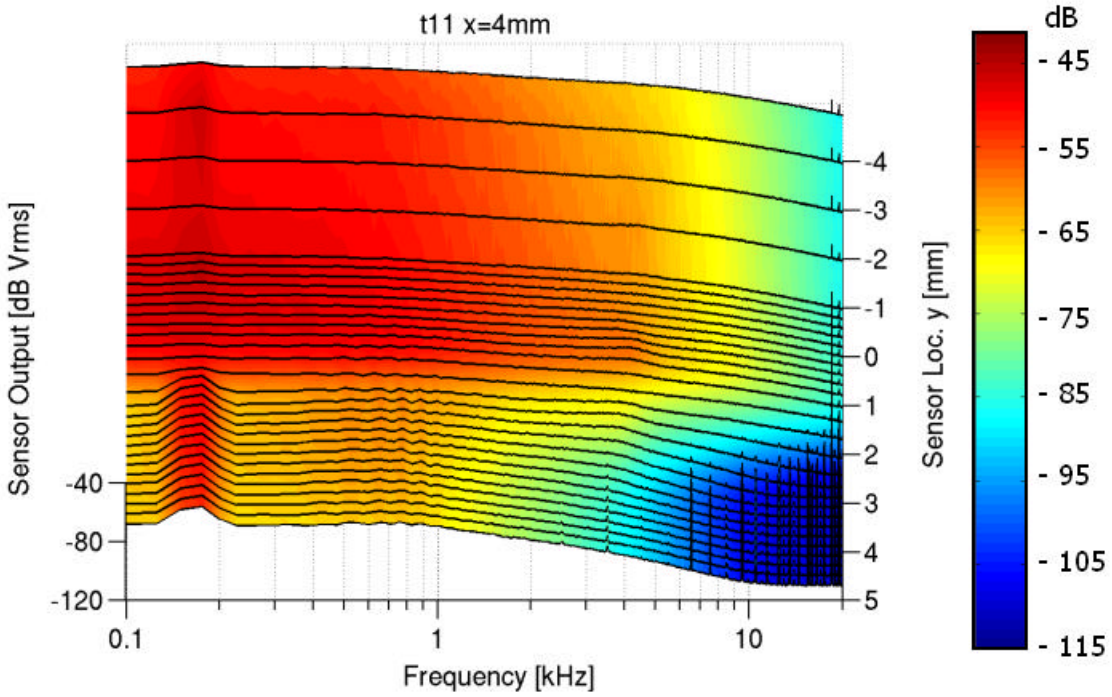

Figure 15: Power spectrum of the hot-wire output for the T11 type at x = 4 mm.

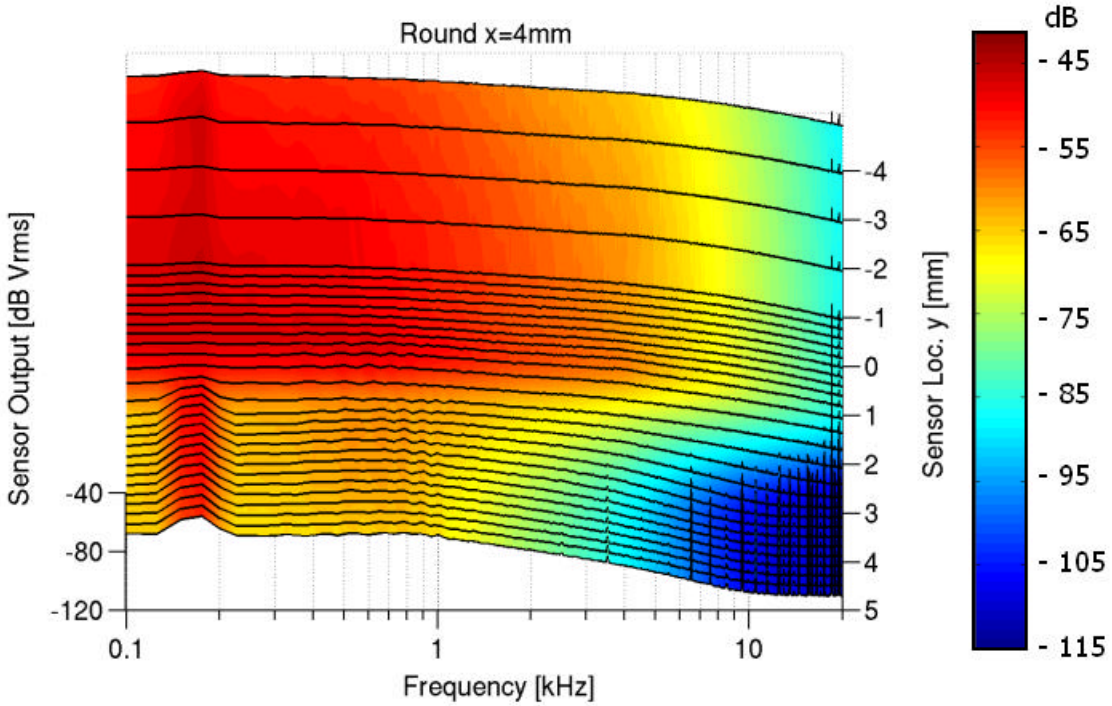

Figure 16: Power spectrum of the hot-wire output for the Round type at x = 4 mm.

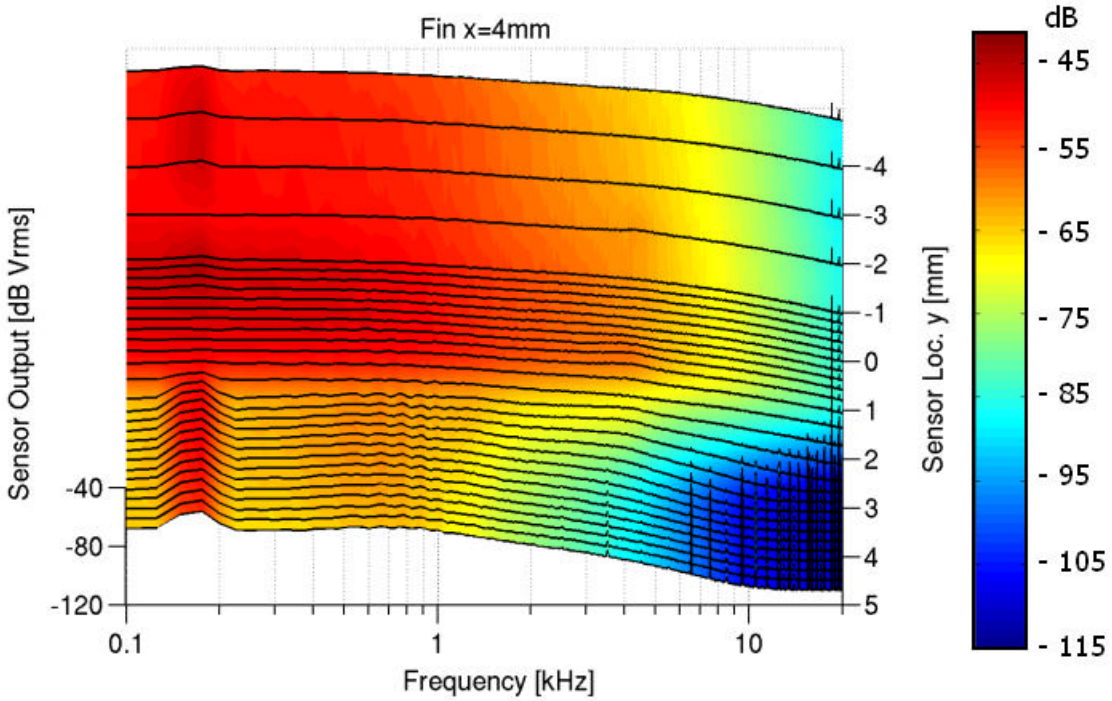

Figure 17: Power spectrum of the hot-wire output for the Fin type at x = 4 mm.

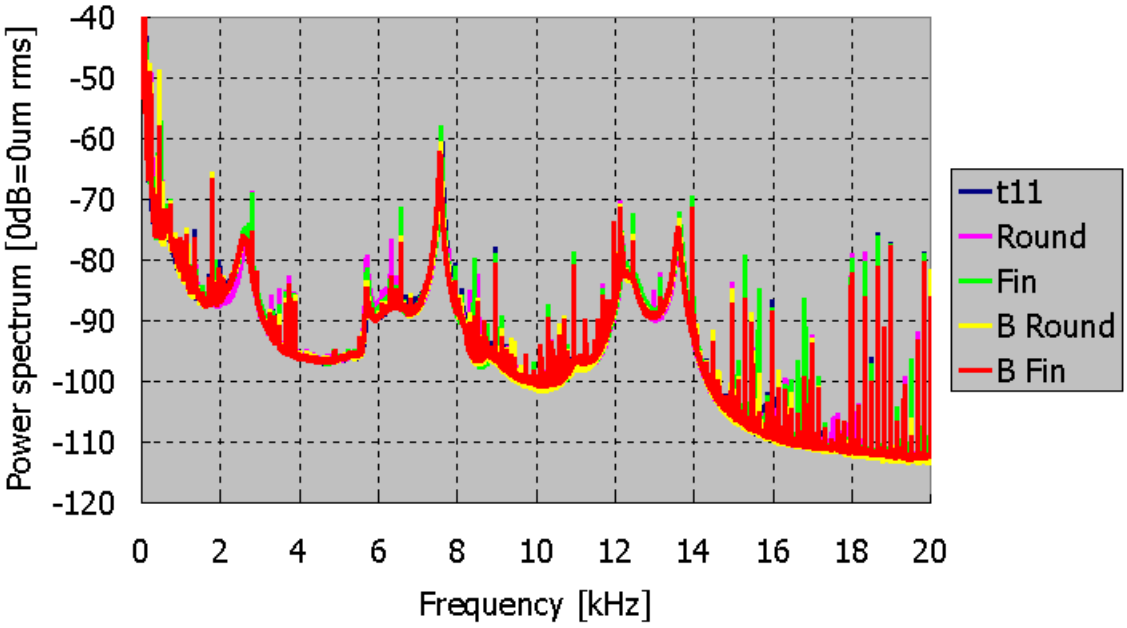

Figure 18: Power spectra of the slider off-track vibration.

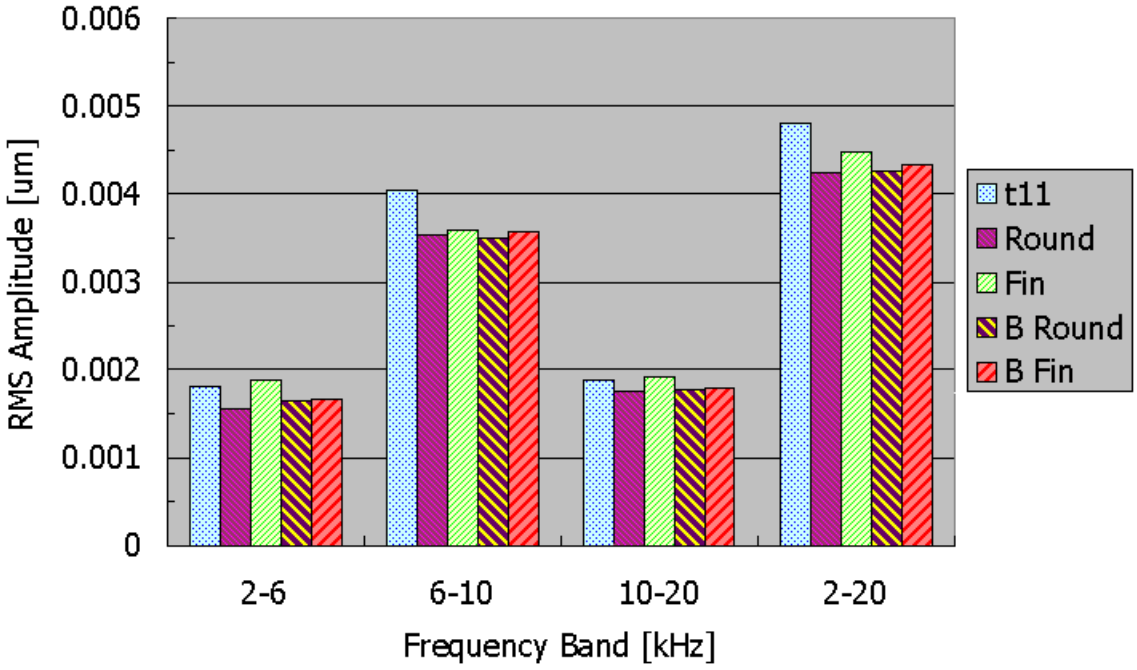

Figure 19: rms vibration amplitudes over several frequency ranges.